Negative Gauge Factor Piezoresistive Composites Based on Polymers Filled with MoS_2 Nanosheets

Sonia Biccai,[1] Conor S. Boland,[1] Daniel P. O'Driscoll,[1] Andrew Harvey,[1] Cian Gabbett,[1] Domhnall R. O'Suilleabhain,[1] Aideen J. Griffin,[1] Zheling Li,[2] Robert J Young,[2] and Jonathan N Coleman[1]*

[1]*School of Physics, CRANN & AMBER Research Centers, Trinity College Dublin, Dublin 2, Ireland*

[2]*National Graphene Institute and School of Materials, The University of Manchester, Manchester, M13 9PL, United Kingdom*

*colemaj@tcd.ie (Jonathan N. Coleman); Tel: +353 (0) 1 8963859.

ABSTRACT: Nanocomposite strain sensors, particularly those consisting of polymer-graphene composites, are increasingly common and are of great interest in the area of wearable sensors. In such sensors, application of strain yields an increase in resistance due to the effect of deformation on inter-particle junctions. Typically, widening of inter-particle separation is thought to increase the junction resistance by reducing the probability of tunnelling between conducting particles. However, an alternative approach would be to use piezoresistive fillers, where an applied strain modifies the intrinsic filler resistance and so the overall composite resistance. Such an approach would broaden sensing capabilities, as using negative piezoresistive fillers could yield strain-induced resistance reductions rather than the usual resistance increases. Here we introduce nanocomposites based on polyethylene-oxide (PEO) filled with MoS_2 nanosheets. Doping of the MoS_2 by the PEO yields nanocomposites which are conductive enough to act as sensors, while efficient stress transfer leads to nanosheet deformation in response to an external strain. The intrinsic negative piezoresistance of the MoS_2 leads to a reduction of the composite resistance on the application of small tensile strains. However, at higher strain the resistance grows due to increases in junction resistance. MoS_2-PEO composite gauge factors are approximately -25 but fall to -12 for WS_2-PEO composites and roughly -2 for PEO filled with $MoSe_2$ or WSe_2. We develop a simple model, which describes all these observations. Finally, we show that these composites can be used as dynamic strain sensors.

KEYWORDS: liquid phase exfoliation; transition metal dichalcogenide; graphene; 2-dimensional; strain gauge;

Over the last decade, the need for next-generation strain and pressure sensors has stimulated a considerable amount of research across many areas of materials science. More recently, demand for wearable sensors which monitor biological functions such as pulse and blood pressure has moved the focus toward soft, flexible sensing materials. This has largely involved the development of nanocomposites and other nanostructured sensing materials.[1-7]

Generally, strain sensors are based on piezoresistive materials, *i.e.* those materials for which an applied strain, ε, results in a resistance change such that

$$\Delta R / R_0 = G\varepsilon \tag{1a}$$

where G is the gauge factor. Usually, the gauge factor is measured at low strain and in that limit it can be shown that[8]

$$G = \frac{1}{\rho_0}\frac{\mathrm{d}\rho}{\mathrm{d}\varepsilon} + (1 + 2\nu) \tag{1b}$$

where ν and ρ are the Poisson ratio and resistivity of the piezoresistive material and ρ_0 is its zero-strain resistivity. For most metals, $\mathrm{d}\rho/\mathrm{d}\varepsilon$ is small, leading to gauge factors in the range 2-4.[8] However, for many semiconducting materials, applying strain leads to changes in band structure that can modify either carrier density or mobility such that $\mathrm{d}\rho/\mathrm{d}\varepsilon$ can be large, resulting in relatively high values of G.[9] For example, *p*-type silicon displays a gauge factor of up to 175.[8] In addition, composite strain sensors based on polymers filled with conductive nano-materials, such as nanotubes or graphene, can display high gauge factors.[10-14] This is generally attributed to quantum mechanical tunnelling between conductive particles which can lead to very high values of $\mathrm{d}\rho/\mathrm{d}\varepsilon$ and so G, as discussed in a number of papers and reviews.[15-17] As an example, polysilicone-graphene composites have recently been reported with gauges factors above 500.[2]

The discussion above implies that piezoresistive materials always have positive gauge factors *i.e.* their resistance increases with increasing tensile strain. While this is true for the vast majority of materials, there exist a small number of materials with negative gauge factors (resistance decreases with increasing tensile strain). Negative piezoresistance is an interesting phenomenon that provides a window into the dependence of band structure on strain and can be harnessed to produce atypical sensors. Notably nickel has a gauge factor of $G = -12$,[8] due to strain-induced conductivity enhancement. Additionally, a small number of semiconductors display negative gauge factors. Most well-known, *n*-type silicon[8] has a negative gauge factor

of –135 while gauge factors as high as –285 have been reported for Si nanowires.[18] In addition, SiC, Ge and GaAs also have reasonably high negative values of G.[8] However, most interestingly for this work is the fact that the band gap of the 2-dimensional semiconductor MoS_2 (*i.e.* the 2H polytype)[19] tends to change with strain,[20-22] leading to negative gauge factors ranging from –225 for bilayer MoS_2 to –50 for few layer MoS_2.[23, 24]

However, with the exception of a handful of reports showing negative gauge factors for polymers filled with Ni particles,[25] nanocomposites have almost universally demonstrated positive G. This is due to the fact that the piezoresistance in composites is dominated by effects associated with inter-particle junctions which lead exclusively to $G > 0$. While polymer fibers coated with conducting polymers have demonstrated small negative gauge factors (due to chain alignment effects),[26, 27] to the best of our knowledge no nanocomposites of polymers filled with semiconducting particles have been reported with negative G. The reason for this is twofold. First, very few researchers have studied the electromechanical properties of polymers filled with semiconducting piezoresistive particles, partly due to the expectation of low conductivity. Secondly, even if such studies were made using negative piezoresistive particles, unless a reasonably strong polymer-particle binding can be achieved, it is difficult to transfer strain to the filler particles. As a result, rather than significantly deforming the filler particles and so reducing the particle resistance, applied strains tend to result in relative motion of adjacent filler particles, leading to increased separation and so enlarged inter-particle junction resistance.[28]

Nevertheless, it would be of basic interest to fabricate negative piezoresistive particle-polymer composites where an applied strain could lead to a reduction in particle resistance. The demonstration of a reduction in overall composite resistance would be an unambiguous indicator of stress/strain transfer at the polymer-particle interface, an area which is of fundamental interest in mechanically reinforced composites[29, 30] (unambiguous because all other piezoresistive effects lead to resistance increases). If strain were transferred, it is likely that the negative piezoresistance of the filler particles could dominate the composite resistance at low strain. However, at higher strain, other more typical effects, such as tunnelling, might dominate, leading to increasing resistance. Such composites would demonstrate interesting and perhaps useful properties such as negative gauge factor, a resistance minimum at some critical strain as well as both positive and negative differential gauge factors, depending on the strain.

In addition, we note that incorporating intrinsically piezoresistive particles in composites has a number of advantages. For example, composite production and processing is cheap and easy

and minimises the content of active materials. In addition, composite formation allows control of the mechanical properties of the sensing material, for example by careful polymer choice, which will be important in bio-medical sensors which sometimes have to be extremely soft. In addition, if one considered non-electrical readout methods (*e.g.* optical *via* photoluminescence), such composites could allow local strain measurements, for example in structural polymers.

We propose that such a material could be fabricated using semiconducting nanosheets of 2D materials such as MoS_2 or WSe_2. 2D materials have generated much interest in recent years due to their shape, aspect ratio and diverse properties.[19, 31] A very wide range of 2D materials, including graphene and MoS_2, can be produced in large quantities by techniques such as liquid exfoliation,[32, 33] allowing the production of a range of structures[34] including polymer-based composites.[35] Furthermore, as mentioned above, MoS_2 is known to demonstrate a negative gauge factor. Negative piezoresistance might be harnessed in a composite because the high aspect ratio of 2D nanosheets may allow the transfer of enough of the applied strain to the nanosheets to yield a significant reduction in nanosheet resistance. If large enough, this could yield a measurable reduction in composite resistance. However, beyond graphene, not many 2D materials have been used as fillers in polymer-based composites. Although a small number of papers have demonstrated mechanical reinforcement in polymer/MoS_2 composites,[36, 37] no papers describe using the semiconducting (2H) form of MoS_2 as a conductive additive while electromechanical studies on 2H-MoS_2 and other semiconducting nanosheet-polymer composites have not been reported.

Here we describe the production of composites fabricated from liquid-exfoliated MoS_2 nanosheets and poly(ethylene oxide) (PEO). We find significant mechanical reinforcement and strain-induced Raman band shifts indicating the transfer of strain from matrix to nanosheet. In addition, we find the PEO dopes the nanosheets, significantly increasing their conductivity and resulting in composite conductivities of $>10^{-5}$ S/m. Most importantly, we find a reduction in resistance at low strain, consistent with the influence of the negative piezoresistive filler, followed by a resistance increase above the yield strain, probably due to tunnelling. We develop a simple model to describe these data that predicts the composite gauge factor to decrease as the nanosheet conductivity increases. Experiments on polymers filled with WS_2, $MoSe_2$ and WSe_2 confirm this prediction. Finally, we have used PEO/MoS_2 composites to demonstrate dynamic strain sensors.

RESULTS AND DISCUSSION

Nanosheet production

MoS_2 nanosheets were produced by liquid phase exfoliation.[38] In brief, MoS_2 powder was sonicated in water and surfactant (sodium cholate) for 330 minutes. The resultant suspension was centrifuged twice[39] to remove both small nanosheets and large unexfoliated crystallites, yielding the larger nanosheets. The optical extinction spectrum of such a size-selected dispersion is shown in figure 1A (black line). The long tail at high wavelength is indicative of scattering as expected for large nanosheets.[40] Using an integrating sphere to remove the scattering spectrum[41] (red line in figure 1A) yields the true absorbance spectrum (blue) which has the shape expected from MoS_2, typified by the A-exciton peak around 670 nm.[41] Using published metrics,[41] we can use this excitonic position as well as the spectral shape to estimate the mean nanosheet thickness and length to be ~5-6 nm and ~240 nm respectively. We can confirm the nature of the nanosheets by performing Raman spectroscopy (λ = 532 nm) on a filtered nanosheet film. As shown in figure 1D, the resultant spectrum shows the characteristic bands at 380 and 405 cm^{-2} as expected for the semiconducting (2H) form of MoS_2.[42]

TEM imaging showed the suspension to contain large numbers of 2D objects which are clearly few-layer nanosheets (figure 1C). Nanosheet lengths as measured from the TEM images are plotted as a histogram in figure 1D. The length distribution varied from 50 nm to 700 nm with a mean at 240 nm. In addition, AFM measurements were performed on nanosheets deposited into Si/SiO_2 with a representative image shown in figure 1E. Statistical analysis (figure 1F) gave a nanosheet length distribution very similar to that measured by TEM as well as a thickness distribution showing the vast majority of nanosheets to be <10 nm thick with a mean at 5.5 nm. This data also shows that 77% of nanosheets were thicker than 4 monolayers and so had roughly thickness-independent bandgaps[43] and so similar (intra) nanosheet conductivities. We note that the length and thickness data extracted from TEM, AFM and spectroscopic data are in good agreement.

Composite fabrication and basic characterisation

Polymer-nanosheet composite suspensions were made by blending the nanosheet dispersion with solutions of poly(ethylene oxide) (PEO) in various ratios to yield a range of mass fractions, M_f, between 0 and 8wt%. These were formed into composite films by dropcasting into petri dishes and oven drying (figure 2A). The resultant composite films appeared completely uniform to the eye. Raman spectroscopy (figure 2B) measured on these films

showed the expected modes from both MoS_2 and PEO, albeit with significantly greater intensity in the MoS_2 modes.

These composites were characterised mechanically by measuring tensile stress-strain curves on at least five samples for each mass fraction. In all cases, ductile behaviour was observed with most breaking strains exceeding 100%. A selection of representative stress-strain curves, focusing on the low-strain region are shown in figure 2C. It is clear from these data that addition of MoS_2 nanosheets tends to stiffen the PEO. This can be seen quantitatively by plotting the average Young's modulus, Y, as a function of MoS_2 volume fraction, ϕ, in figure 2D. This shows a considerable increase from Y=270 MPa for PEO to Y=570 MPa for the ϕ = 0.5% (2 wt%) sample, after which the modulus saturates. Such a saturation at higher filler loading is usually attributed to aggregation effects.[44] In addition, we found that the ultimate tensile strength did not change significantly with nanosheet loading, staying roughly constant at 10-15 MPa, whereas the yield strain fell significantly from ~10% for PEO to ~4% for a composite with 2.5 vol% (10 wt%) MoS_2.

We can analyse the modulus increase quantitatively using the rule of mixtures. This model predicts the composite modulus, Y, to increase with filler volume fraction as:[45]

$$Y = \eta_L \eta_o Y_F \phi + Y_P (1-\phi) \qquad (2)$$

where ϕ is the filler volume, Y_F and Y_P are the moduli of the filler and the polymer respectively and η_L, and η_o are efficiency factors associated with filler length and orientation respectively (for randomly oriented distributions of platelets,[46] η_o = 8/15). This model matches the data very well up to $\phi \approx$ 0.5%, after which the modulus diverges from theory. Such divergence is often found in nanocomposites and is usually attributed to aggregation effects as mentioned above.[44] The linear fit gives $\eta_L \eta_o Y_F$ =60 GPa, which, combined with the value of η_o given above and the known value of Y_F=270 GPa,[47] yields η_L =0.4. This value is considerably larger than the expected value (η_L<0.1, see SI), implying that the reinforcement is considerably better than might be expected. This might be explained by crystallisation of PEO at the MoS_2 surface, a process that is known to boost reinforcement.[48] Such crystallisation may indeed occur as PEO is known to crystallise on the surface of graphene.[49] In any case, the relatively high levels of reinforcement indicate that stress is transferred effectively across the PEO/MoS_2 interface. This in turn implies that the MoS_2 nanosheets come under strain as the polymer is stretched.

We also measured the electrical conductivity of the composites as a function of MoS_2 loading as shown in figure 2E. We found the conductivity to increase from ~10^{-6} S/m for the lowest volume fraction to ~2×10^{-5} S/m for the ϕ = 1.75% sample. Interestingly, these values are significantly higher than typically reported values of the conductivity of MoS_2 nanosheet-only films (~10^{-6} S/m)[50, 51] which is very surprising as we would expect mixing with polymer to reduce the conductivity compared to neat nanosheet networks.

To understand this further we fitted the conductivity data to percolation theory:[52, 53]

$$\sigma = \sigma_0 \left(\phi - \phi_c\right)^n \quad (4)$$

where σ_0 is approximately the conductivity of a film of the filler material alone (*i.e.* an MoS_2 nanosheet network),[34] ϕ_c is the percolation threshold (*i.e.* the volume fraction where the first conductive path is formed) and n is the percolation exponent. The fit is shown as the solid line in figure 2E and yields the parameters $\phi_c = 10^{-3}$, n = 1.1 and σ_0 = 1.73 mS/m. For randomly arranged 2D fillers, percolation thresholds are typically $\phi_c \sim t_{NS}/l_{NS}$, predicting $\phi_c \sim 0.02$ here. The experimental value is significantly below this prediction, possibly due to aggregation-induced network formation, often referred to as kinetic percolation.[54] In addition, the exponent is slightly lower than the value of 1.3 expected for percolation in two dimensions (*i.e.* a thin film), although reduced n-values often accompany low percolation thresholds.[53]

What is most unusual about the electrical data is the relatively high value of σ_0. This parameter is a measure of the conductivity of a polymer-free network of the nanoconductor.[34, 55] The conductivities of networks of MoS_2 nanosheets are, however, typically found to be ~10^{-6}-10^{-5} S/m,[34, 55] considerably lower than the value of σ_0 quoted above. To explain this discrepancy, we hypothesise that the PEO dopes the MoS_2 nanosheets *via* a charge transfer mechanism, as is found to occur in some polymer/MoS_2 combinations.[56] To test this we deposited two MoS_2-only networks on electrode arrays, measuring the conductivity to be 3×10^{-5} S/m in each case. Then, a ~1 μL droplet of a 25 g/L aqueous PEO solution was deposited on each network. They were then fully dried and the conductivity re-measured. This procedure was repeated twice more with the conductivities plotted in figure 2E inset. In both cases, we observed a steady increase in conductivity with an ×10 increase observed after three droplets. This is a good indication that contact with PEO results in a significant increase in carrier density of the nanosheets.

Electromechanical properties of MoS_2/PEO composites

What is most interesting about these composites, however, is their electromechanical response. Shown in figure 3A are typical plots of fractional resistance change, $\Delta R/R_0$, as a function of tensile, uniaxial strain, ε. It is clear from these data that the resistance falls at low strain, reaches a minimum at intermediate strains before increasing at higher strains, usually reaching resistances somewhat higher than the zero-strain resistance. This behaviour was observed for all samples tested (47) over all MoS_2 mass fractions. The negative resistances changes were quite stable over time as demonstrated by step-strain measurements (see SI). Such strain-induced reductions in resistance are extremely unusual, with almost all nanocomposite electromechanical data showing monotonic resistance-strain increases. The only exception we are aware of is our own paper which showed an unusual polysilicone/graphene composite to undergo a resistance increase followed by a subsequent decrease with increasing strain.[2] However, in that case, the unusual behaviour was attributed to dynamic behaviour associated with the extreme softness of the matrix.

In terms of quantitative characterisation, the simplest aspect of this behaviour is the gauge factor, G (the slope of $\Delta R/R_0$ *vs.* ε, measured in the limit of low strain). As shown in figure 3B, the mean gauge factors measured for MoS_2/PEO composites are all negative and range between −12 and −25 with a peak at intermediate loading (which will be discussed below). As mentioned above, this is in contrast to carbon nanotube- or graphene-filled composites which always show positive G (typically $2 < G < 200$).[57] However, they are similar to previous results for composites of polysilicone filled with 1D nickel structures which showed negative gauge factors as large as -40.[25]

To try to understand this interesting and unusual behaviour, we first note that, as shown in figure 3C, the strain associated with the resistance minimum appears to coincide with the yield strain (strain at maximum stress) as measured in the tensile mechanical tests. As shown in figure 3D, this correlation appeared to hold over all samples. This implies that the negative gauge factor is associated (at least in part) with the elastic regime while plastic deformation at higher strains results in large resistance increases.

Normally, tensile deformation of composites results in relative motion of the conductive filler particles. This can result in an increase in inter-particle separation with strain, leading to a reduction in inter-particle tunnelling, and so in increase in overall composite resistance. A mechanism such as this is likely to be responsible for the resistance increase above the yield strain. However, below the yield strain the resistance decrease likely has its origin in the fact

that the MoS_2 nanosheets themselves have a negative gauge factor as described above.[24] Given the mechanical results shown in figure 2D, it is likely that, at low strains within the elastic region, enough stress is transferred to the MoS_2 nanosheets to stretch them, thus reducing the nanosheet resistance. This then leads to a reduction in composite resistance.

As mentioned above, in standard composite strain sensors, the composite piezoresistance is rarely due to the piezoresistance of the filler particles themselves, but rather is associated with effects such as changes in the inter-nanosheet tunnelling resistance.[2] This is because the relatively low resistance of the filler particles themselves means the overall conductivity is limited by junction resistances.[58] Thus, any strain-induced changes in the filler-particle resistance would be swamped by changes in inter-nanosheet tunnelling with strain. This is not, however, the case in MoS_2-filled composites because the nanosheets themselves are much more resistive than conductive fillers such as graphene nanosheets or carbon nanotubes. The composite resistance is then likely to be limited by the nanosheet resistance rather than the inter-nanosheet junction resistance, allowing strain-induced changes in nanosheet resistance to yield changes in composite resistance.

For this hypothesis to be true, enough stress must be transferred from polymer to nanosheet to stretch the nanosheets. As mentioned above, the reasonably-high measured reinforcement indicates this to be possible. To test for transfer of applied strain to the MoS_2 nanosheets, we performed Raman spectroscopy as a function of strain applied to the composite as a whole. We found both the E^1_{2g} and A_{1g} bands to downshift as a result of the applied strain. This is a clear sign that the MoS_2 nanosheets themselves are being stretched with the nanocomposite film. The in-plane vibrational E^1_{2g} mode with a wavenumber of ~ 380 cm^{-1}, has a shift rate of about -0.7 $cm^{-1}/\%$. Although this value is lower than reported values of -1 $cm^{-1}/\%$,[59] one needs to bear in mind that the reported values were from more 'ideal' specimen of either mechanically exfoliated flakes or CVD-grown flakes which are larger, thinner and aligned in the plane of strain. From previous experience with graphene, it is not surprising that the smaller, thicker and randomly-oriented few-layer MoS_2 flakes used in this work have lower absolute shift rates. In contrast, the shift rate of the out-of-plane A_{1g} mode is -0.96 $cm^{-1}/\%$, only slightly lower than the values reported for few-layer flakes,[59] presumably because the shift rate of this mode is less sensitive to flake size. It should also be pointed out that the linearity between the Raman bands position and the strain only holds until ~ 0.5% strain. After that it flattens, indicating a lower interfacial stress transfer efficiency.

The confirmation that strain can be transferred to the MoS_2 nanosheets, makes it likely that the observed negative composite gauge factor is associated with stretching of the nanosheets themselves. Because the initial resistance decrease is followed by an increase at high strain, a physical model is needed to fully describe the system. Here we develop such a model.

Modelling Composite Piezoresistance

We begin by noting that the conductivity any network of nanosheets, whether a solution-deposited porous network or a network embedded in a polymer matrix, depends effectively on four factors: the intrinsic nanosheet resistance, the inter-nanosheet junction resistance, the network structure and the nanosheet dimensions. While a full description of the electrical properties of networks is complicated,[60] we have argued that the network resistivity can be approximately described by (see ref[2], supporting information):

$$\rho = \left(R_{NS} + R_J \right) \chi / l_{NS} \qquad (5)$$

where R_{NS} and R_J are the nanosheet and junction resistance, l_{NS} is the nanosheet length and χ incorporates all effects of the network structure. This simple model is based on the idea that every time a charge carrier passes through a nanosheet, it must also traverse an inter-nanosheet junction. In addition, the factor of l_{NS} incorporates the minimum number of nanosheets per conductive path (*i.e.* L/l_{NS}, where L is the sample length). In general, R_{NS} and R_J, and so ρ, will all depend on applied strain. We note that equations 4 and 5 must be closely related. Because equation 4 describes the ϕ-dependence of the conductivity, one of the terms in equation 5 must also display ϕ-dependence. Because χ is a measure of the nanosheet network structure, this parameter must be ϕ-dependent. As a result, the simplest way to rationalise equation 5 with equation 4 is to write $\chi \propto \left(\phi - \phi_c \right)^{-n}$.

Then, equation 1a can be modified to represent the nanosheet: $R_{NS}(\varepsilon) = R_{NS,0} G_{NS} \varepsilon + R_{NS,0}$, where G_{NS} is the intrinsic gauge factor of the nanosheet and the subscript zero represents zero-strain. Assuming isostrain (*i.e.* the strain in the nanosheet is equal to the applied strain which is a basic assumption in most simple models of composite mechanics, *e.g.* the rule of mixtures[61]), we can write:

$$\rho(\varepsilon) = \left[R_{NS,0} \left(G_{NS} \varepsilon + 1 \right) + R_J(\varepsilon) \right] \chi / l_{NS} \qquad (6)$$

where $R_{NS,0}$ is the zero-strain nanosheet resistance.

In addition, we note that for any incompressible material the fractional resistance change in response to strain is found by combining equations 1a and 1b and taking $\nu = 0.5$:

$$\frac{\Delta R}{R_0} = \left[\frac{1}{\rho_0} \frac{\mathrm{d}\rho}{\mathrm{d}\varepsilon} + 2 \right] \varepsilon \tag{7}$$

Combining equations 6 and 7 yields

$$\frac{\Delta R}{R_0} = \left[\frac{G_{NS} + (\mathrm{d}R_J / \mathrm{d}\varepsilon) / R_{NS,0}}{1 + R_{J,0} / R_{NS,0}} + 2 \right] \varepsilon \tag{8}$$

where $R_{J,0}$ is the zero-strain junction resistance.

This is a general equation which describes the electromechanical response of a network. It contains three terms representing (from left to right) the effect of strain on the resistance of the filler particles, the junction resistance and the geometry of the composite as a whole.

To quantify the second term, we initially used two pre-existing models, based on tunnelling[28] and dynamic network connectivity[2] to estimate $\mathrm{d}R_J / \mathrm{d}\varepsilon$. In both cases, we obtained an equation that matches experimental data qualitatively *(i.e.* yielding an initial decrease in $\Delta R/R_0$, followed by an increase at higher strain). However, we note that the strain-dependence of conductivity/resistivity in composites is quite complicated; including contributions from tunnelling, network connectivity as well as orientation effects. Thus, we decided to take an empirical approach to identify a function to approximately represent the dependence of R_J on strain without specifying any particular mechanism. To do this, we prepared a PEO-graphene composite, which should display no negative piezoresistance, and whose strain-dependent resistance should be controlled by the same factors controlling the high-strain behaviour in these PEO-MoS_2 composites. We measured the strain dependent resistance (see SI), finding behaviour which was consistent with equation 8, combined with the following empirical function:

$$\frac{\mathrm{d}R_J}{\mathrm{d}\varepsilon} = \frac{k\varepsilon}{\varepsilon_1 + \varepsilon} \tag{9}$$

where k and ε_1 are constants. It must be emphasised that equation 9 can only be considered strictly true for PEO-based composites. For other matrices, it would be necessary to identify a suitable function in a manner described above. We note that the integral of this particular expression is approximately given by $R_J \sim k\varepsilon^2 / (2\varepsilon_1 + \varepsilon)$.

Combining these equations yields a semi-empirical model that describes the strain dependence of the composite resistance:

$$\frac{\Delta R}{R_0} = \left[\frac{G_{NS} + a\varepsilon / (\varepsilon_1 + \varepsilon)}{1 + R_{J,0} / R_{NS,0}} + 2 \right] \varepsilon \qquad (10)$$

where $a = k / R_{NS,0}$ is a constant. This equation has been found to fit very well to all experimental $\Delta R / R_0$ *vs.* ε data as shown (solid lines) in figure 3A. It is worth noting that the obtainable fit parameters (other than those representing the low-strain slope) are not of significant interest here. The value of this equation lies in its ability to demonstrate that the data can be explained by a combination of strain-induced deformation of the nanosheets (at low strain) coupled with strain-induced modification of the junction resistance (dominant at high strain).

Most importantly, once we accept the validity of equation 10, we can use it to analyse the composite gauge factor data. By definition, the gauge factor is measured at low strain. Taking the limit of equation 10 at low strain yields

$$\frac{\Delta R}{R_0} = \left[\frac{G_{NS}}{1 + R_{J,0} / R_{NS,0}} + 2 \right] \varepsilon \qquad (11)$$

which is equivalent to writing

$$G = \frac{G_{NS}}{1 + R_{J,0} / R_{NS,0}} + 2 \qquad (12)$$

Assuming G_{NS} is constant, this equation implies that the volume fraction dependence of G shown in figure 3B is associated with variation of $R_{J,0} / R_{NS,0}$ with ϕ. Assuming that $G_{NS} = -50$,[24] we can use this equation to calculate $R_{J,0} / R_{NS,0}$, which we plot *versus* ϕ in figure 3F. There are two things to note. First, the nanosheet resistance is similar to the junction resistance in all cases. This justifies our initial assumption that the junction resistance is not the sole effective limiting factor in the composite electrical properties. Secondly, the variation in $R_{J,0} / R_{NS,0}$ with ϕ implies the network structure changes slightly with nanosheet loading. However, the increase in $R_{J,0}$ with ϕ at low loading levels is not in agreement with tunnelling models,[28] which would predict the inter-particle separation, and hence $R_{J,0}$, to fall with ϕ. However, we note that tunnelling models can only describe some of the effects contributing to

strain dependent conductivity changes in composites. In addition to changes in tunnelling probability, we would expect changes in network connectivity and nanosheet orientation-distribution effects as strain is applied. We suggest that it is this combination of various factors which results in these counter-intuitive results. Secondly, it is interesting that the data shows a peak in $R_{J,0}$ to occur at $\phi \approx 0.5\%$, very close to the loading level where aggregation starts to occur (figure 2D), indicating that the network structure is dependent on the aggregation state.

This near parity between nanosheet and junction resistance allows us to roughly predict the junction resistance by estimating the nanosheet resistance. Previously,[51] the mobility of an MoS_2 nanosheet network was measured to be ~0.15 cm^2/Vs. Combining this with the conductivity of a PEO-doped nanosheet network, taken from σ_0 = 1.73 mS/m, allows us to estimate the carrier density in the nanosheets used here to be ~4×10^{20} m^{-3}. Ref [51] also measured the intrinsic nanosheet mobility to be ~50 cm^2/Vs. Assuming the carrier density of an individual nanosheet to be similar to the network allows us to estimate the nanosheet conductivity to be σ_{NS}~0.5 S/m. Modelling the nanosheets as squares with thickness t_{NS} gives a nanosheet resistance of $R_{NS,0} = l_{NS} / (\sigma_{NS} l_{NS} t_{NS}) = (\sigma_{NS} t_{NS})^{-1}$. Using the estimated value of σ_{NS} and the measured nanosheet thickness (~5.5 nm) yields $R_{NS,0}$~400 MΩ. Because of the similarity between nanosheet and junction resistances mentioned above, this implies the inter-MoS_2 nanosheet junction resistance to be of a similar order. It is reasonable to believe that junction resistances of this magnitude may also apply to other 2D materials. It is worth noting that these junction resistances are considerably larger than values of ~MΩ reported for nanotube-nanotube junctions,[58] probably due to trapping of polymer between nanosheets.

Negative gauge factors in composites of PEO and other 2D materials

If the junction resistance is roughly invariant with nanoheet type, it implies that other, more conductive 2D materials should yield less negative composite gauge factors even if the intrinsic gauge factors were approaching that for MoS_2 (*i.e.* −50). The reason for this is that, if the nanosheet conductivity increases without significant changes to the junction resistance, this will lead to a scenario where $R_{J,0} >> R_{NS,0}$ so that changes to $R_{NS,0}$ under strain have very little effect on the composite resistance.

To test this, we prepared PEO composites filled with nanosheets of WS_2, $MoSe_2$ and WSe_2, as well as graphene for comparison, all at the same nanosheet volume fraction of 0.12 vol%. As shown previously, the intrinsic conductivity of these TMDs varies significantly because of

differences in their bandgaps.[50] We performed resistance-strain measurements (figure 4A), extracting both conductivity and gauge factor for the composites. In addition, we note that the data can be well-fit by equation 10. As shown in figure 4B, we find the gauge factor to become less negative as the composite conductivity increases. In addition, we find the graphene-based composite to have a positive gauge factor as expected.[62]

We can understand this in more detail by developing a simple model. First we modify equation 5 to represent the zero-strain situation (*i.e.* $\rho_0 = \left(R_{NS,0} + R_{J,0}\right)\chi / l_{NS} = 1/\sigma$, where σ is the composite conductivity at zero-strain) and then combine with equation 12 to find a relationship between *G* and σ which we can apply to the TMD-based composites (graphene has a different, positive value of G_{NS})[62]:

$$G = 2 + G_{NS}\left(1 - \frac{\chi_{0.12\%} R_{J,0}\sigma}{l_{NS}}\right) \qquad (13)$$

where $\chi_{0.12\%}$ indicates the measurements were made for composites of nanosheet volume fraction of 0.12%. This equation supports the suggestion made above that, for PEO-based composites, more conductive composites have reduced gauge factors simply because lower nanosheet resistance increases the relative importance of the junction resistance. Under these circumstances, strain-induced changes to nanosheet resistance have limited effect on the overall composite resistance.

Negative G strain sensors

The electromechanical response shown in figure 3A means these composites can be used as strain sensors. For most of the composites, the *R*-ε curves were approximately linear up to at least 5% strain (figure 3D), making these sensors appropriate for low-strain sensing. To demonstrate this, we applied sinusoidal strains varying from ε_{Min} = 0.5% to ε_{Max} = 2% with frequencies of 0.1, 0.5 and 1 Hz as shown in figure 5 A-C (top row). In each case, the resultant resistance trace followed a roughly harmonic response that was out-of-phase with the applied strain (see figure 5A-C lower panels). This is what is expected for a negative *G* material and is in contrast with typical composite strain sensors which show resistance traces that are in-phase with the applied stain.

To demonstrate the consistency of the data, we show Fourier transforms calculated from the entire duration of the resistance traces in figure 5 D-F (durations: 100 s for 0.1 Hz, 200 s for 0.5 Hz and 50 s for 1 Hz). In all cases, a clear peak is observed superimposed on a 1/*f*

background. As illustrated by the arrows, the main peaks are at the expected frequencies of 0.1, 0.5 and 1 Hz.

CONCLUSIONS

In summary, we prepared composites of the polymer PEO and liquid-exfoliated MoS_2 nanosheets. We found the polymer to dope the nanosheets, increasing their conductivity and resulting in composites which were more conductive than might have been expected. Nanosheet addition also resulted in composite reinforcement, with stiffness more than doubling at ~0.5 vol.-% MoS_2, indicative of good polymer-nanosheet stress transfer. As a direct result of this stress transfer, applying strain to the composite results in straining of the nanosheets themselves. Because of the negative gauge factor of MoS_2 itself, this resulted in a reduction in nanosheet, and so composite, resistance at low strain. In addition, we observed a resistance increase above the yield strain, which we attribute to a mechanism such as tunnelling. We have developed a simple model which describes the data. Among other things this model predicts the composite gauge factor (measured at low strain) to be smaller for composites filled with semiconducting nanosheets of higher conductivity and by comparing the piezorestance performance of PEO filled with MoS_2, WS_2, $MoSe_2$ and WSe_2 we observed such behaviour. Finally, we demonstrate that such composites can be used as dynamic strain sensors, measuring low-strain periodic deformations. This work significantly broadens the range of phenomena observed in the area of piezoresistive composites. We believe these observations represent interesting materials physics combining standard composite physics with the more unusual piezoresistive properties of networks.

METHODS

Materials and Methods

Polyethylene oxide (PEO, MW: 100000, CAS number: 25322-68-3), Molybdenum disulphide (MoS_2, 99%, CAS number: 1317-33-5), Tungsten disulphide (WS_2, 99%, CAS number: 12138-09-9), and Sodium cholate hydrate (SC, ≥ 97% dried material, CAS number: 206986-87-0) were purchased from Sigma Aldrich. Molybdenum diselenide ($MoSe_2$, 99.9%, CAS number: 12058-18-3) was purchased from Alfa Aesar, Tungsten diselenide (WSe_2, 99.8%, CAS number, 12067-46-8) was purchased from Fisher Scientific Ltd and Graphite (Grade: 3763) was purchased from Asbury Graphite Mills. Each product was used as received. MoS_2, WS_2, $MoSe_2$, WSe_2 and graphene nanosheets were prepared *via* liquid phase exfoliation. TMDs and

graphite powder (20 g/L) were sonicated in water for 1 hour using a solid flathead tip (Sonics VX-750) at 60% amplitude with a pulse of 6 s on and 2 s off duty cycle. The dispersion was centrifuged for 2 hours at 6000 RPM to separate low-mass impurities into the supernatant using a Hettich Mikro 220R centrifuge with a fixed-angle rotor 1016. The supernatant was discarded and the sediment re-dispersed in 2 g/L sodium cholate aqueous solution by sonication for 330 minutes using the same sonic tip settings as previous. Afterwards, large nanosheets were selected in the supernatant by centrifuging at 1000 RPM to remove large unexfoliated material into the sediment.

Optical characterisation of nanosheet dispersions was performed in a 4 mm path quartz cuvette using a UV-vis spectrophotometer (Perkin Elmer Lambda 650). Raman analyses were performed with a Horiba Jobin Yvon LabRAM HR800 (100× objective lens, travel spot size ~ 1 μm, λ = 532) under ambient conditions. TEM analyses were performed on dispersions using a JEOL 2100, operated at 200 kV with holey carbon grids being used as substrates. SEM analyses were performed on composite PEO/MoS_2 films using a SEM Carl Zeiss Ultra operating at 2 kV.

A Veeco Nanoscope-IIIa system (Digital Instruments) was used in tapping mode AFM measurements. Samples were prepared by drop casting 15 μL of diluted dispersion (O.D. approx. 0.4) onto a preheated, cleaned Si/SiO_2 (285 mn oxide layer) at 180°C. Wafers were washed with water to remove excess surfactant. Individually nanosheets were then analysed using previously established length corrections for pixilation effects and tip broadening.[41] Step height analysis was used to convert the apparent thickness of nanosheets to the number of layers using a step height of 1.9 nm.[41] The nanosheet thickness was then found by multiplying the number of monolayers per nanosheet by 0.6 nm.

Film preparation

Polymer-nanosheet composite films with various mass fractions were prepared. Specific volumes of nanosheet dispersions were mixed with PEO powder. Water was added, keeping the total volume constant (15 mL), and the dispersion nanosheet-polymer was poured into a Petri dish and dried overnight at 50 °C. The films obtained appeared uniform to the eye.

Electromechanical Testing

Composite films were cut and uniform strips were obtained (width = 2.25 mm; thickness ~ 70 μm each strip). The strips were attached to the clamps of the tensile tester at a distance of 9.73 mm apart. Simultaneously, the clamps were connected to a source meter for electrical

measurements. Electrical analysis on composites films were executed using a Keithley KE2601 source meter using a 2-probe configuration to measure DC current under typical applied voltages of 40V. All measurements were made in ambient conditions. Electromechanical measurements were performed using the Keithley KE2601 source meter in conjunction with a Zwick Z0.5 Pro-Line Tensile Tester (100 N Load Cell) controlled using labview software. For all samples made, zero-strain conductivity was measured before measuring the tensile strain. Afterwards, the samples were strained (10 mm/min speed test) and both stress and resistance of the samples were recorded. From the stress-strain curves it was possible to evaluate the Young's moduli using TestXpert software. Using R-ε curves, it was possible to plot $\Delta R/R_0$ *versus* strain and by evaluating the slope of the graph G values were extrapolated. A sine wave simulation program was used in order to execute cyclic tests on 0.5 wt.-% PEO/MoS_2 films. The dynamic strain profile was obtained performing the test at 3 different frequencies (0.1, 0.5 and 1 Hz) at a gauge length of 9.73 mm for 500 cycles. A minimum number of 7 tests per sample was performed then the average and standard deviation was calculated using Origin software.

In-situ Raman deformation test

The specimen was prepared by drop casting the 0.5 wt.-% MoS_2/PEO mixture solution onto PMMA beam and left to dry. Prior to the deposition, the PMMA beams were UV treated to improve adhesion. The PMMA beam with the MoS_2/PEO nanocomposite film on top was placed on the microscope stage of Raman spectrometer (LabRAM HR Evolution, Horiba) equipped with laser (λ = 488 nm). The sample was deformed step-wise using a four-point bending rig with the strain measured by a strain gauge next to the film.[63]

SUPPORTING INFORMATION: The Supporting Information is available free of charge on the ACS Publications website: detailed analysis of nanosheet dispersions; information on electromechanical data; Identification of function relating R_J to ε.

ACKNOWLEDGEMENTS: We acknowledge the European Union under grant agreements n°785219 Graphene Flagship-core 2 and the European Research Council Advanced Grant (FUTURE-PRINT). Additional support was provided by Science Foundation Ireland (SFI/12/RC/2278).

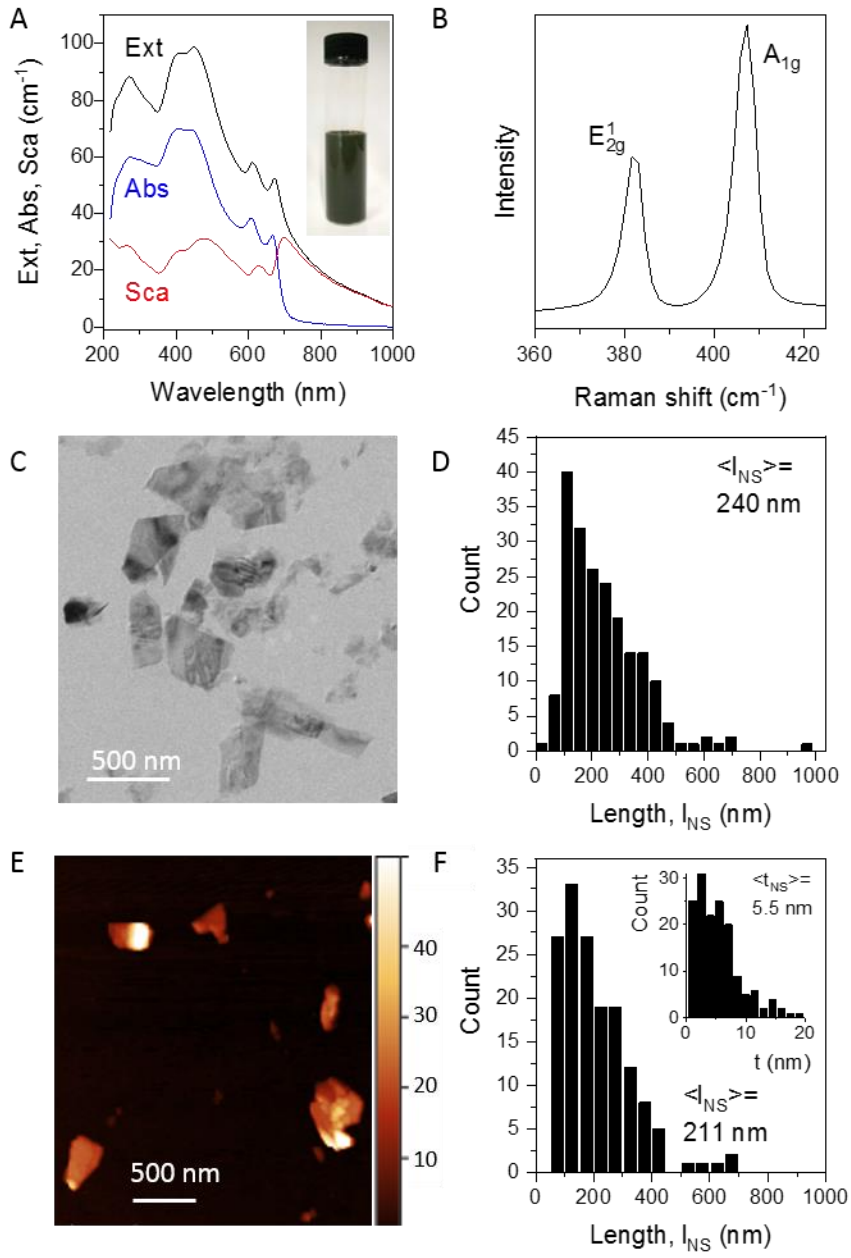

Figure 1: Characterisation of liquid exfoliated nanosheets. A) Inset: Photograph of dispersion of MoS_2 nanosheets. Main panel: Optical extinction, scattering and absorption spectra, measured on a dispersion of liquid exfoliated MoS_2 nanosheets. B) Raman spectrum (532 nm) measured on a film of MoS_2 nanosheets. C) Representative TEM image showing liquid exfoliated MoS_2 nanosheets. D) Nanosheet length (longest dimension) histogram, measured from TEM images (200 counts). E) Representative AFM image of liquid exfoliated MoS_2 nanosheets deposited on Si/SiO_2. F) Nanosheet length and thickness (inset) histograms, measured from AFM images (155 counts).

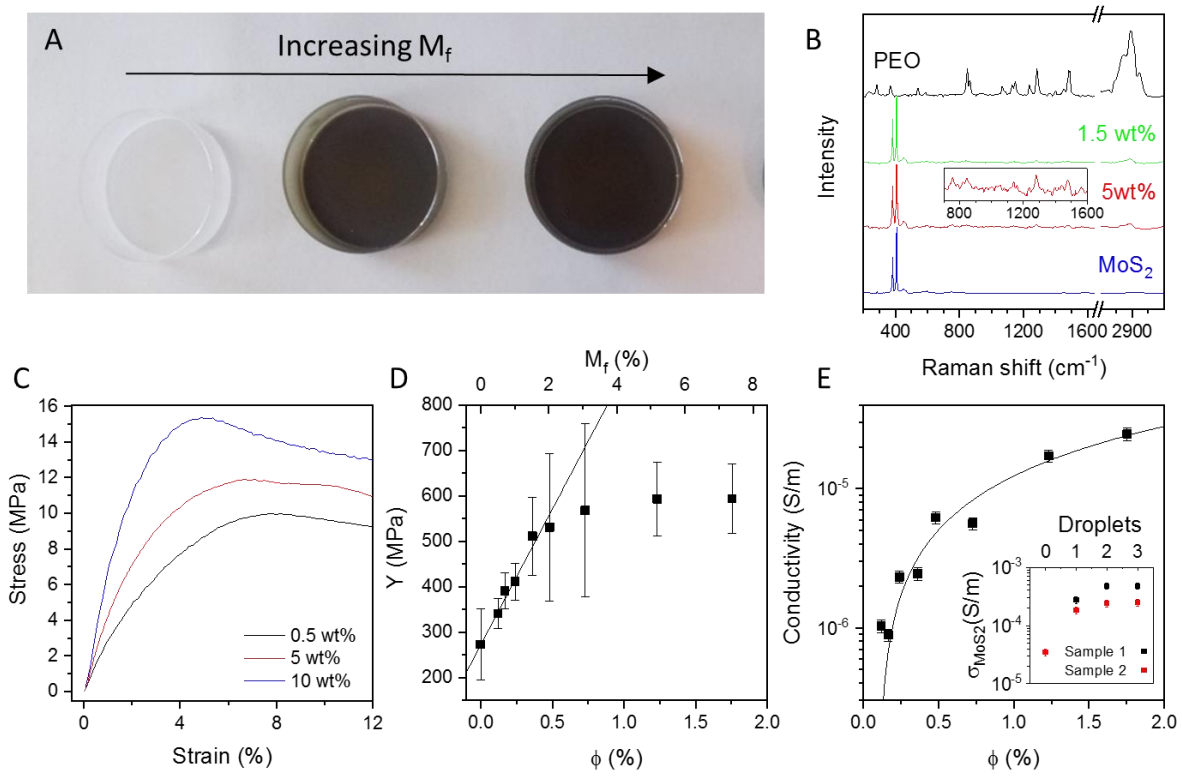

Figure 2: Basic characterisation of MoS_2/PEO composites. A) Photograph of PEO (left) and MoS_2/PEO films having dried in petri dishes. B) Raman spectra measured on a PEO film and MoS_2/PEO composite films with M_f = 1.5 and 5 wt.-%. Also shown is the spectrum associated with an MoS_2-only film. The inset shows PEO modes are also observed in the composite films. C) Representative stress-strain curves for selected MoS_2/PEO composites. D) Young's modulus plotted *versus* MoS_2 volume fraction for MoS_2/PEO composites. Each datum is an average of 6-11 individual measurements. The top axis shows the approximate mass fraction. The line is a fit to shear lag theory (eq 2&3). E) Conductivity plotted *versus* MoS_2 volume fraction for MoS_2/PEO composites. The line is a fit to percolation theory (eq 4). Inset: Conductivity of an MoS_2-only network before (0 droplets) and after depositing 1, 2 and 3 droplets of PEO dissolved in water.

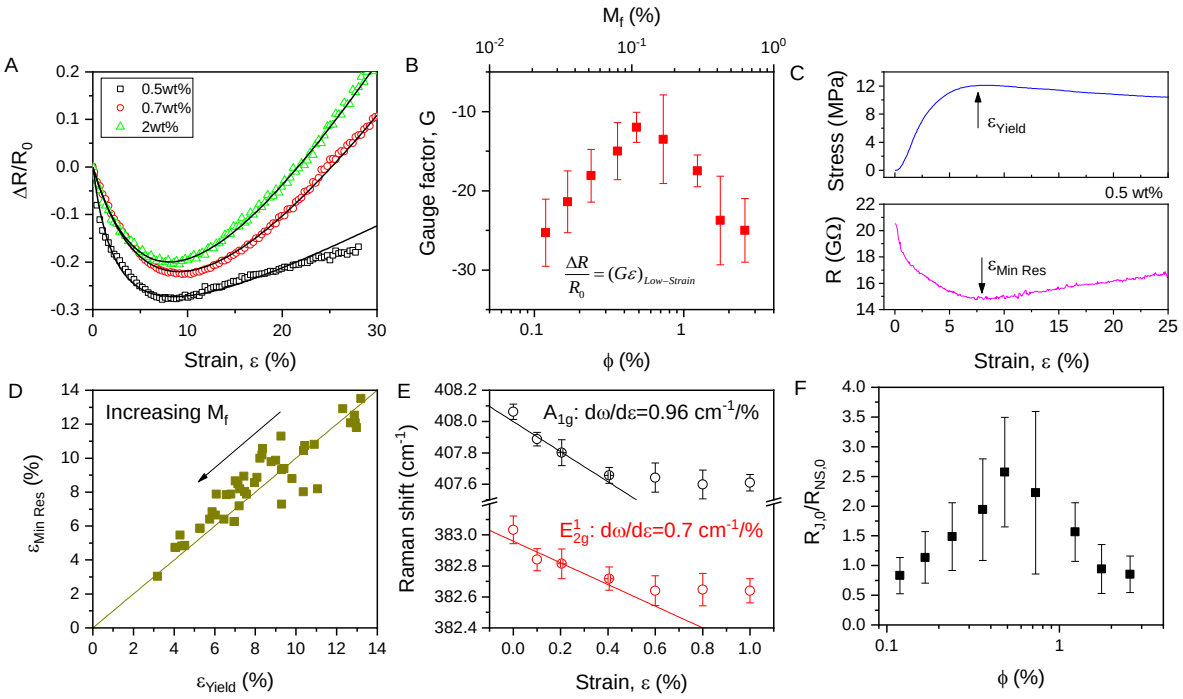

Figure 3: Electromechanical properties of MoS_2/PEO composites. A) Representative curves showing fractional resistance change as a function of applied tensile strain. The lines are fits to equation 10. B) Gauge factor extracted from curves such as those in A (*i.e.* slope at low strain). The data represent mean and standard error calculated from > 6 independent measurements. C) Typical stress-strain (top) and resistance-strain (bottom) curves measured for plotted MoS_2/PEO composites (here $M_f = 0.5\%$). The arrows define the maximum and minimum points as plotted in D. D) Strain associated with resistance minimum plotted *versus* the strain associated with the stress maximum (*i.e.* the yield strain) for all MoS_2/PEO composites (see C for definition). E) The Raman band position of E^1_{2g} and A_{1g} bands as the function of strain. The measurement is the average from 7 measurements, and the error bars represent the standard error of the mean. F) Ratio of zero-strain junction resistance to zero-strain nanosheet resistance calculated using eq 12 and plotted *versus* ϕ. The error bars combine the error in G with an assumption that the error in G_{NS} is ±10.

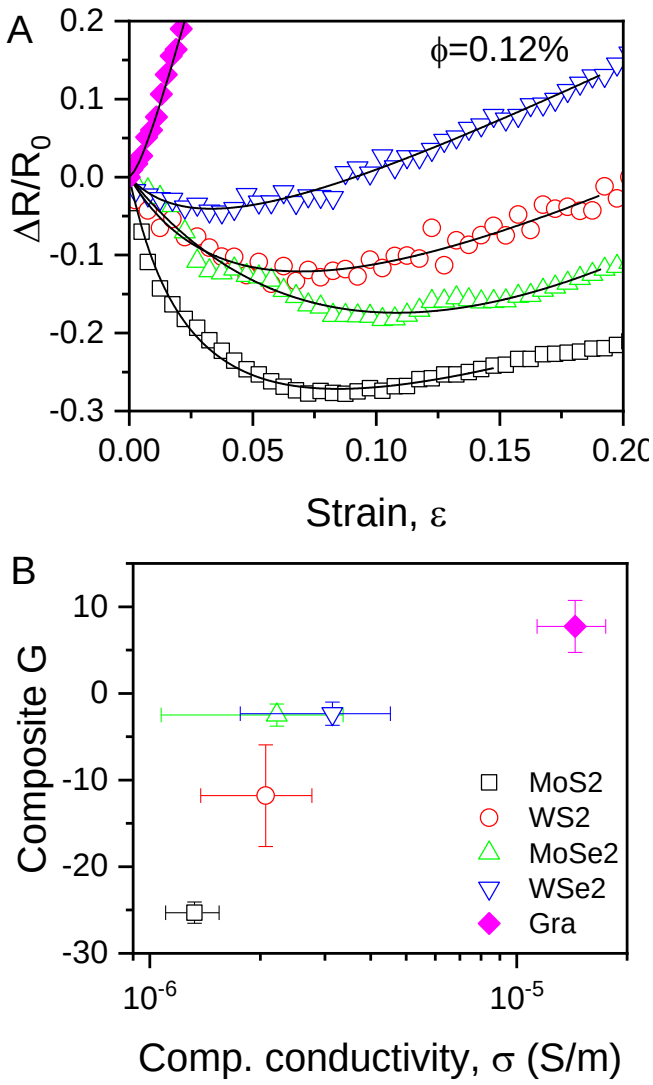

figure 4: A) Representative resistance-strain curves for composites of PEO filled with 4 different types of TMD nanosheet as well as graphene (all at ϕ = 0.12vol%). The lines are fits to equation 10. B) Gauge factors for the composites shown in A, plotted *versus* measured composite conductivity. Each point is an average over >5 measurements. The colour coding used in B also applied to A.

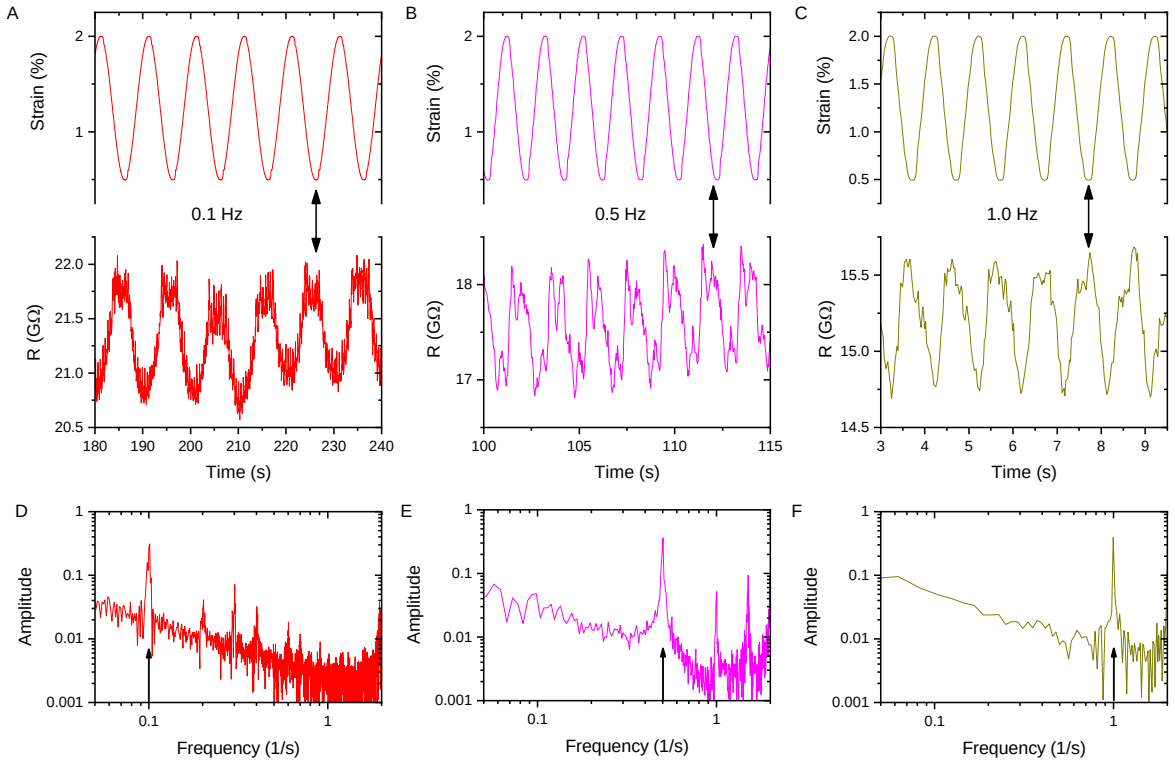

Figure 5: Dynamic strain sensing with MoS_2/PEO composites (M_f = 0.5 wt.-%). The top row shows dynamic strain profiles oscillating at three different frequencies: A) 0.1 Hz, B) 0.5 Hz and C) 1 Hz. The bottom row shows the resultant resistance response. D-F) Fourier transforms for the *R-t* curves in A-C. The arrows indicate the main peak with the other peaks representing harmonics.

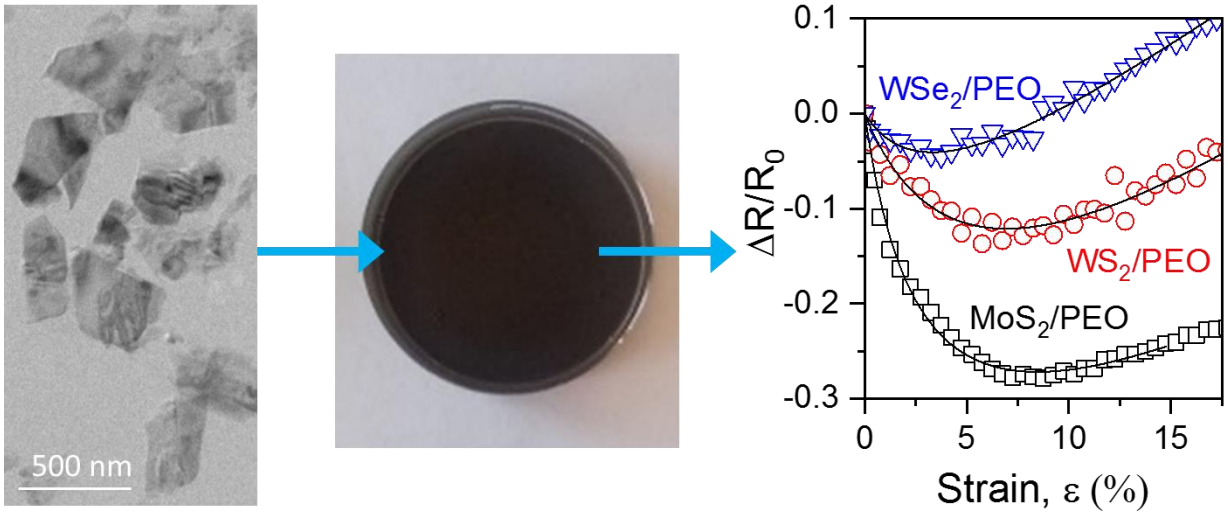

ToC fig

References

1. Amjadi, M.; Kyung, K. U.; Park, I.; Sitti, M., Stretchable, Skin-Mountable, and Wearable Strain Sensors and Their Potential Applications: A Review. *Adv. Funct. Mater.* **2016,** 26, 1678-1698.
2. Boland, C. S.; Khan, U.; Ryan, G.; Barwich, S.; Charifou, R.; Harvey, A.; Backes, C.; Li, Z.; Ferreira, M. S.; Mobius, M. E.; Young, R. J.; Coleman, J. N., Sensitive Electromechanical Sensors Using Viscoelastic Graphene-Polymer Nanocomposites. *Science* **2016,** 354, 1257-1260.
3. Pang, C.; Lee, G. Y.; Kim, T. I.; Kim, S. M.; Kim, H. N.; Ahn, S. H.; Suh, K. Y., A Flexible and Highly Sensitive Strain-Gauge Sensor Using Reversible Interlocking of Nanofibres. *Nat. Mater.* **2012,** 11, 795-801.
4. Wang, X. W.; Gu, Y.; Xiong, Z. P.; Cui, Z.; Zhang, T., Silk-Molded Flexible, Ultrasensitive, and Highly Stable Electronic Skin for Monitoring Human Physiological Signals. *Adv. Mater.* **2014,** 26, 1336-1342.
5. Casiraghi, C.; Macucci, M.; Parvez, K.; Worsley, R.; Shin, Y.; Bronte, F.; Borri, C.; Paggi, M.; Fiori, G., Inkjet Printed 2D-Crystal Based Strain Gauges on Paper. *Carbon* **2018,** 129, 462-467.
6. Smith, A. D.; Niklaus, F.; Paussa, A.; Schroder, S.; Fischer, A. C.; Sterner, M.; Wagner, S.; Vaziri, S.; Forsberg, F.; Esseni, D.; Ostling, M.; Lemme, M. C., Piezoresistive Properties of Suspended Graphene Membranes under Uniaxial and Biaxial Strain in Nanoelectromechanical Pressure Sensors. *ACS Nano* **2016,** 10, 9879-9886.
7. Large, M. J.; Ogilvie, S. P.; Meloni, M.; Graf, A. A.; Fratta, G.; Salvage, J.; King, A. A. K.; Dalton, A. B., Functional Liquid Structures by Emulsification of Graphene and Other Two-Dimensional Nanomaterials. *Nanoscale* **2018,** 10, 1582-1586.
8. Fiorillo, A. S.; Critello, C. D.; Pullano, S. A., Theory, Technology and Applications of Piezoresistive Sensors: A Review. *Sens. Actuators, A* **2018,** 281, 156-175.
9. Barlian, A. A.; Park, W. T.; Mallon, J. R.; Rastegar, A. J.; Pruitt, B. L., Review: Semiconductor Piezoresistance for Microsystems. *Proc. IEEE* **2009,** 97, 513-552.
10. Abshirini, M.; Charara, M.; Liu, Y. T.; Saha, M.; Altan, M. C., 3d Printing of Highly Stretchable Strain Sensors Based on Carbon Nanotube Nanocomposites. *Adv. Eng. Mater.* **2018,** 20.
11. Christ, J. F.; Aliheidari, N.; Ameli, A.; Potschke, P., 3d Printed Highly Elastic Strain Sensors of Multiwalled Carbon Nanotube/Thermoplastic Polyurethane Nanocomposites. *Mater. Des.* **2017,** 131, 394-401.
12. Lu, Y.; Biswas, M. C.; Guo, Z. H.; Jeon, J. W.; Wujcik, E. K., Recent Developments in Bio-Monitoring *via* Advanced Polymer Nanocomposite-Based Wearable Strain Sensors. *Biosens. Bioelectron.* **2019,** 123, 167-177.
13. Ye, X. L.; Yuan, Z.; Tai, H. L.; Li, W. Z.; Du, X. S.; Jiang, Y. D., A Wearable and Highly Sensitive Strain Sensor Based on a Polyethylenimine-RGO Layered Nanocomposite Thin Film. *J. Mater. Chem. C* **2017,** 5, 7746-7752.
14. Chen, Y.; Potschke, P.; Pionteck, J.; Voit, B.; Qi, H. S., Smart Cellulose/Graphene Composites Fabricated by *in situ* Chemical Reduction of Graphene Oxide for Multiple Sensing Applications. *J. Mater. Chem. C.* **2018,** 6, 7777-7785.
15. Hu, N.; Karube, Y.; Yan, C.; Masuda, Z.; Fukunaga, H., Tunneling Effect in a Polymer/Carbon Nanotube Nanocomposite Strain Sensor. *Acta Mater.* **2008,** 56, 2929-2936.
16. Alamusi; Hu, N.; Fukunaga, H.; Atobe, S.; Liu, Y. L.; Li, J. H., Piezoresistive Strain Sensors Made from Carbon Nanotubes Based Polymer Nanocomposites. *Sensors* **2011,** 11, 10691-10723.

17. Stassi, S.; Cauda, V.; Canavese, G.; Pirri, C. F., Flexible Tactile Sensing Based on Piezoresistive Composites: A Review. *Sensors* **2014,** 14, 5296-5332.
18. Lugstein, A.; Steinmair, M.; Steiger, A.; Kosina, H.; Bertagnolli, E., Anomalous Piezoresistance Effect in Ultrastrained Silicon Nanowires. *Nano Lett.* **2010,** 10, 3204-3208.
19. Chhowalla, M.; Shin, H. S.; Eda, G.; Li, L. J.; Loh, K. P.; Zhang, H., The Chemistry of Two-Dimensional Layered Transition Metal Dichalcogenide Nanosheets. *Nature Chem.* **2013,** 5, 263-275.
20. Castellanos-Gomez, A.; Roldan, R.; Cappelluti, E.; Buscema, M.; Guinea, F.; van der Zant, H. S. J.; Steele, G. A., Local Strain Engineering in Atomically Thin MoS2. *Nano Lett.* **2013,** 13, 5361-5366.
21. Conley, H. J.; Wang, B.; Ziegler, J. I.; Haglund, R. F.; Pantelides, S. T.; Bolotin, K. I., Bandgap Engineering of Strained Monolayer and Bilayer MoS2. *Nano Lett.* **2013,** 13, 3626-3630.
22. Nayak, A. P.; Pandey, T.; Voiry, D.; Liu, J.; Moran, S. T.; Sharma, A.; Tan, C.; Chen, C. H.; Li, L. J.; Chhowalla, M.; Lin, J. F.; Singh, A. K.; Akinwande, D., Pressure-Dependent Optical and Vibrational Properties of Mono Layer Molybdenum Disulfide. *Nano Lett.* **2015,** 15, 346-353.
23. Tsai, M. Y.; Tarasov, A.; Hesabi, Z. R.; Taghinejad, H.; Campbell, P. M.; Joiner, C. A.; Adibi, A.; Vogel, E. M., Flexible MoS2 Field-Effect Transistors for Gate-Tunable Piezoresistive Strain Sensors. *ACS Appl. Mater. Interfaces* **2015,** 7, 12850-12855.
24. Manzeli, S.; Allain, A.; Ghadimi, A.; Kis, A., Piezoresistivity and Strain-Induced Band Gap Tuning in Atomically Thin MoS2. *Nano Lett.* **2015,** 15, 5330-5335.
25. Johnson, O. K.; Kaschner, G. C.; Mason, T. A.; Fullwood, D. T.; Hansen, G., Optimization of Nickel Nanocomposite for Large Strain Sensing Applications. *Sens. Actuators, A* **2011,** 166, 40-47.
26. Seyedin, S.; Zhang, P.; Naebe, M.; Qin, S.; Chen, J.; Wang, X. A.; Razal, J. M., Textile Strain Sensors: A Review of the Fabrication Technologies, Performance Evaluation and Applications. *Materials Horizons* **2019,** 6, 219-249.
27. Wu, J.; Zhou, D.; Too, C. O.; Wallace, G. G., Conducting Polymer Coated Lycra. *Synth. Met.* **2005,** 155, 698-701.
28. Rahman, R.; Servati, P., Effects of Inter-Tube Distance and Alignment on Tunnelling Resistance and Strain Sensitivity of Nanotube/Polymer Composite Films. *Nanotechnology* **2012,** 23.
29. Young, R. J.; Gong, L.; Kinloch, I. A.; Riaz, I.; Jalil, R.; Novoselov, K. S., Strain Mapping in a Graphene Monolayer Nanocomposite. *ACS Nano* **2011,** 5, 3079-3084.
30. Li, Z. L.; Young, R. J.; Kinloch, I. A., Interfacial Stress Transfer in Graphene Oxide Nanocomposites. *ACS Appl. Mater. Interfaces* **2013,** 5, 456-463.
31. Wang, Q. H.; Kalantar-Zadeh, K.; Kis, A.; Coleman, J. N.; Strano, M. S., Electronics and Optoelectronics of Two-Dimensional Transition Metal Dichalcogenides. *Nat. Nanotechnol.* **2012,** 7, 699-712.
32. Bonaccorso, F.; Bartolotta, A.; Coleman, J. N.; Backes, C., 2D-Crystal-Based Functional Inks. *Adv. Mater.* **2016,** 28, 6136-6166.
33. Nicolosi, V.; Chhowalla, M.; Kanatzidis, M. G.; Strano, M. S.; Coleman, J. N., Liquid Exfoliation of Layered Materials. *Science* **2013,** 340, 1226419.
34. Gabbett, C.; Boland, C. S.; Harvey, A.; Vega-Mayoral, V.; Young, R. J.; Coleman, J. N., The Effect of Network Formation on the Mechanical Properties of 1D:2D Nano:Nano Composites. *Chem. Mater.* **2018,** 30, 5245-5255.
35. Young, R. J.; Kinloch, I. A.; Gong, L.; Novoselov, K. S., The Mechanics of Graphene Nanocomposites: A Review. *Compos. Sci. Technol.* **2012,** 72, 1459-1476.

36. Feng, X. M.; Wang, X.; Xing, W. Y.; Zhou, K. Q.; Song, L.; Hu, Y., Liquid-Exfoliated MoS2 by Chitosan and Enhanced Mechanical and Thermal Properties of Chitosan/MoS2 Composites. *Compos. Sci. Technol.* **2014,** 93, 76-82.
37. Zhou, K. Q.; Jiang, S. H.; Bao, C. L.; Song, L.; Wang, B. B.; Tang, G.; Hu, Y.; Gui, Z., Preparation of Poly(Vinyl Alcohol) Nanocomposites with Molybdenum Disulfide (Mos2): Structural Characteristics and Markedly Enhanced Properties. *RSC Adv.* **2012,** 2, 11695-11703.
38. Niu, L. Y.; Coleman, J. N.; Zhang, H.; Shin, H.; Chhowalla, M.; Zheng, Z. J., Production of Two-Dimensional Nanomaterials *via* Liquid-Based Direct Exfoliation. *Small* **2016,** 12, 272-293.
39. Backes, C.; Szydlowska, B. M.; Harvey, A.; Yuan, S. J.; Vega-Mayoral, V.; Davies, B. R.; Zhao, P. L.; Hanlon, D.; Santos, E. J. G.; Katsnelson, M. I.; Blau, W. J.; Gadermaier, C.; Coleman, J. N., Production of Highly Monolayer Enriched Dispersions of Liquid-Exfoliated Nanosheets by Liquid Cascade Centrifugation. *ACS Nano* **2016,** 10, 1589-1601.
40. Harvey, A.; Backes, C.; Boland, J. B.; He, X. Y.; Griffin, A.; Szydlowska, B.; Gabbett, C.; Donegan, J. F.; Coleman, J. N., Non-Resonant Light Scattering in Dispersions of 2D Nanosheets. *Nature Commun.* **2018,** 9, 4553.
41. Backes, C.; Smith, R. J.; McEvoy, N.; Berner, N. C.; McCloskey, D.; Nerl, H. C.; O'Neill, A.; King, P. J.; Higgins, T.; Hanlon, D.; Scheuschner, N.; Maultzsch, J.; Houben, L.; Duesberg, G. S.; Donegan, J. F.; Nicolosi, V.; Coleman, J. N., Edge and Confinement Effects Allow *in situ* Measurement of Size and Thickness of Liquid-Exfoliated Nanosheets. *Nature Commun.* **2014,** 5, 4576.
42. Lee, C.; Yan, H.; Brus, L. E.; Heinz, T. F.; Hone, J.; Ryu, S., Anomalous Lattice Vibrations of Single- and Few-Layer MoS2. *ACS Nano* **2010,** 4, 2695-2700.
43. Mak, K. F.; Lee, C.; Hone, J.; Shan, J.; Heinz, T. F., Atomically Thin MoS2: A New Direct-Gap Semiconductor. *Phys. Rev. Lett.* **2010,** 105, 4.
44. Papageorgiou, D. G.; Kinloch, I. A.; Young, R. J., Mechanical Properties of Graphene and Graphene-Based Nanocomposites. *Prog. Mater. Sci.* **2017,** 90, 75-127.
45. Young, R. J.; Liu, M. F.; Kinloch, I. A.; Li, S. H.; Zhao, X.; Valles, C.; Papageorgiou, D. G., The Mechanics of Reinforcement of Polymers by Graphene Nanoplatelets. *Compos. Sci. Technol.* **2018,** 154, 110-116.
46. Li, Z. L.; Young, R. J.; Wilson, N. R.; Kinloch, I. A.; Valles, C.; Li, Z., Effect of the Orientation of Graphene-Based Nanoplatelets Upon the Young's Modulus of Nanocomposites. *Compos. Sci. Technol.* **2016,** 123, 125-133.
47. Bertolazzi, S.; Brivio, J.; Kis, A., Stretching and Breaking of Ultrathin MoS2. *ACS Nano* **2011,** 5, 9703-9709.
48. Coleman, J. N.; Cadek, M.; Ryan, K. P.; Fonseca, A.; Nagy, J. B.; Blau, W. J.; Ferreira, M. S., Reinforcement of Polymers with Carbon Nanotubes. The Role of an Ordered Polymer Interfacial Region. Experiment and Modeling. *Polymer* **2006,** 47, 8556-8561.
49. Tong, Y.; Lin, Y.; Wang, S. D.; Song, M., A Study of Crystallisation of Poly (Ethylene Oxide) and Polypropylene on Graphene Surface. *Polymer* **2015,** 73, 52-61.
50. Cunningham, G.; Hanlon, D.; McEvoy, N.; Duesberg, G. S.; Coleman, J. N., Large Variations in Both Dark- and Photoconductivity in Nanosheet Networks as Nanomaterial Is Varied from MoS2 to WTe2. *Nanoscale* **2015,** 7, 198-208.
51. Kelly, A. G.; Hallam, T.; Backes, C.; Harvey, A.; Esmaeily, A. S.; Godwin, I.; Coelho, J.; Nicolosi, V.; Lauth, J.; Kulkarni, A.; Kinge, S.; Siebbeles, L. D. A.; Duesberg, G. S.; Coleman, J. N., All-Printed Thin-Film Transistors from Networks of Liquid-Exfoliated Nanosheets. *Science* **2017,** 356, 69-72.
52. McLachlan, D. S.; Sauti, G., The AC and DC Conductivity of Nanocomposites. *J. Nanomater.* **2007**.

53. Bauhofer, W.; Kovacs, J. Z., A Review and Analysis of Electrical Percolation in Carbon Nanotube Polymer Composites. *Compos. Sci. Technol.* **2009,** 69, 1486-1498.
54. Kovacs, J. Z.; Mandjarov, R. E.; Blisnjuk, T.; Prehn, K.; Sussiek, M.; Muller, J.; Schulte, K.; Bauhofer, W., On the Influence of Nanotube Properties, Processing Conditions and Shear Forces on the Electrical Conductivity of Carbon Nanotube Epoxy Composites. *Nanotechnology* **2009,** 20.
55. Liu, Y. P.; He, X. Y.; Hanlon, D.; Harvey, A.; Khan, U.; Li, Y. G.; Coleman, J. N., Electrical, Mechanical, and Capacity Percolation Leads to High-Performance MoS2/Nanotube Composite Lithium Ion Battery Electrodes. *ACS Nano* **2016,** 10, 5980-5990.
56. Hong, S.; Yoo, G.; Kim, D. H.; Song, W. G.; Le, O. K.; Hong, Y. K.; Takahashi, K.; Omkaram, I.; Son, D. N.; Kim, S., The Doping Mechanism and Electrical Performance of Polyethylenimine-Doped MoS2 Transistor. In *Physica Status Solidi C: Current Topics in Solid State Physics, Vol 14 No 3-4*, Hildebrandt, S.; VonGraberg, T.; Hopcke, H.; Ma, L.; Panarina, N.; Perelaer, J.; Zastrow, M.; Perets, E., Eds. 2017; Vol. 14, p 1600262.
57. Boland, C. S.; Khan, U.; Backes, C.; O'Neill, A.; McCauley, J.; Duane, S.; Shanker, R.; Liu, Y.; Jurewicz, I.; Dalton, A. B.; Coleman, J. N., Sensitive, High-Strain, High-Rate Bodily Motion Sensors Based on Graphene-Rubber Composites. *ACS Nano* **2014,** 8, 8819-8830.
58. Nirmalraj, P. N.; Lyons, P. E.; De, S.; Coleman, J. N.; Boland, J. J., Electrical Connectivity in Single-Walled Carbon Nanotube Networks. *Nano Lett.* **2009,** 9, 3890-3895.
59. McCreary, A.; Ghosh, R.; Amani, M.; Wang, J.; Duerloo, K. A. N.; Sharma, A.; Jarvis, K.; Reed, E. J.; Dongare, A. M.; Banerjee, S. K.; Terrones, M.; Namburu, R. R.; Dubey, M., Effects of Uniaxial and Biaxial Strain on Few-Layered Terrace Structures of MoS2 Grown by Vapor Transport. *ACS Nano* **2016,** 10, 3186-3197.
60. O'Callaghan, C.; da Rocha, C. G.; Manning, H. G.; Boland, J. J.; Ferreira, M. S., Effective Medium Theory for the Conductivity of Disordered Metallic Nanowire Networks. *Phys. Chem. Chem. Phys.* **2016,** 18, 27564-27571.
61. Hull, D.; Clyne, T. W., *An Introduction to Composite Materials*. Cambridge University Press: Cambridge, 1996.
62. Yokaribas, V.; Wagner, S.; Schneider, D. S.; Friebertshauser, P.; Lemme, M. C.; Fritzen, C. P., Strain Gauges Based on CVD Graphene Layers and Exfoliated Graphene Nanoplatelets with Enhanced Reproducibility and Scalability for Large Quantities. *Sensors* **2017,** 17, 17.
63. Li, Z. L.; Kinloch, I. A.; Young, R. J.; Novoselov, K. S.; Anagnostopoulos, G.; Parthenios, J.; Galiotis, C.; Papagelis, K.; Lu, C. Y.; Britnell, L., Deformation of Wrinkled Graphene. *ACS Nano* **2015,** 9, 3917-3925.